Journal of Solar Energy Research (JSER)

Journal homepage: www.jser.ut.ac.ir

An Explainable Image-Derived Illumination Non-Uniformity Index for Photovoltaic Attenuation Estimation

Mothiga Shivani J*, Ashok Kumar B, Senthilrani S

Department of Electrical and Electronics Engineering, Thiagarajar College of Engineering, Tamil Nadu, India

ARTICLE INFO

Article Type:

Research Article

Received:2026.06.17
Accepted in revised form:2026.07.29

Keywords:
Photovoltaic panels; Illumination non-uniformity; Image-based attenuation estimation; Partial shading; Frequency-domain image analysis; Non-intrusive monitoring

A B S T R A C T

Partial shading caused by dust accumulation, surface contaminants, and nearby obstructions reduces the incident irradiance on photovoltaic (PV) modules, leading to significant performance degradation. Conventional approaches for assessing shading effects rely on electrical measurements, irradiance sensors, or model-based calibration, increasing system complexity and limiting scalability. Although image-processing techniques have been widely investigated for PV inspection, most existing studies emphasize qualitative fault identification rather than quantitative attenuation assessment. This paper presents a non-intrusive image-processing framework that interprets PV panel images as two-dimensional illumination fields and introduces an Illumination Non-Uniformity Index (INUI) derived from physically interpretable spatial and frequency-domain descriptors. The proposed index integrates global intensity variation, spatial discontinuity, and low-frequency illumination distortion to characterize diverse shading patterns. An image-derived attenuation metric is subsequently established to quantify attenuation severity, demonstrating a monotonic relationship with illumination non-uniformity without requiring learning-based models, electrical measurements, or irradiance sensors. Experimental evaluation under diverse shading conditions confirms consistent monotonic behaviour, robustness against imaging variations, and computational efficiency suitable for large-scale visual inspection. The proposed framework provides an explainable, lightweight, and scalable methodology for quantitative image-based assessment of shading-induced attenuation in photovoltaic modules, offering a practical alternative for visual condition monitoring and supporting future intelligent PV inspection systems.

1. Introduction

The use of photovoltaic power generation has become a vital part of the energy systems of the modern world because of its environmental advantages and scalability. The performance of photovoltaic panels is, however, highly sensitive to non-uniform illumination caused by dust and surface contaminant accumulation, bird droppings, and neighbouring obstructions. These conditions create spatial irradiance variations that lead to power attenuation and reduced energy efficiency. Accurate

*Corresponding Author Email: mothigashivani@student.tce.edu

Cite this article: J,M S , B,A K and S,S . (2026). An Explainable Image-Derived Illumination Non-Uniformity Index for Photovoltaic Attenuation Estimation. Journal of Solar Energy Research, 11(3), 3252-3266. doi: 10.22059/jser.2026.416342.1760

DOI: 10.22059/jser.2026.416342.1760

©The Author(s). Publisher: University of Tehran Press.

assessment of illumination-induced performance degradation is therefore important for performance analysis, maintenance scheduling, and operational monitoring of photovoltaic systems. Recent studies have demonstrated the growing potential of non-intrusive image-based methods for PV panel inspection. Image-processing techniques supported by deep learning have been used to identify cracks in PV modules with high accuracy [1] and to model energy loss due to shadows in solar arrays [2]. Monitoring of the cleanliness of PV panels and the severity of soiling has also been investigated by means of aerial and ground-based imaging and images at the visible spectrum [3]. Image based classification of soiled PV modules has been applied to robotic cleaning systems to enable automated maintenance [4] and optical transmittance-based image classification has been suggested to measure dust deposition on PV panels [5]. Besides the process of dirt and the outer surface, image-based and machine learning methods have been applied to fault detection and diagnosis in the PV systems. Real-time fault detection has utilized hybrid machine learning models [6] and a review of the literature has highlighted challenges in soiling estimation, including environmental variability and data dependency [7]. Photovoltaic array fault diagnosis using modulated photocurrent signals has also been studied by applying machine learning techniques [8], and automated PV fault detection by deep learning-based image classification frameworks has been studied [9]. More sophisticated configurations that comprise convolutional and recurrent neural networks have enhanced the fault diagnosis capability with highly challenging working environments [10].

A thorough assessment of soiling and shading has been made possible by cell-level and drone-based inspection techniques as sophisticated imaging systems with high resolution become more widely available. There have been reports of cell-resolved soiling measurement with drone imagery showing an improvement in spatial resolution of degradation analysis [11] and a use of visible-spectrum imaging and machine learning in detecting PV module soiling in real-world case scenarios [12]. Fast partial shading detection and estimation of power loss ratio at the module level has also been suggested by use of digital image processing methods [13]. The results of partial shading on the performance of PV panels have also been confirmed using experimental studies [14]. The traditional PV fault diagnostic techniques have always been based on the electrical measurements and the analysis of characteristic curves. The detection of faults using the simulated and experimentally determined current–voltage (I–V) curves has been explored in order to identify an abnormal operating condition [15]. Unmanned aerial vehicles (UAVs) have also been used in thermographic inspection of PV plants on large scale, though numerous operational and practical issues have been encountered with regard to cost, complexity and environmental dependence [16].

In addition to visible inspection, electroluminescence inspection has been an extensively reviewed defect inspection method. Autonomous multi-defect segmentation of electroluminescence images of PV modules has been developed based on deep learning frameworks [17], and fault detection based on learning systems has been applied to solar energy system using high-dimensional feature representation [18]. RGB image analysis has also been used for the automatic assessment of soiling and partial shading on photovoltaic panels [19]. Although these developments have occurred, various investigations have highlighted difficulties revolving around PV soiling supervision and performance evaluation, especially scalable, inexpensive, and explicable answers [20]. PV module cell analysis Image segmentation has been suggested as a tool to aid defect localization [21], and convolutional and recurrent neural network structures have been applied to identify faults in PV arrays [22]. Previous modelling work had aimed at the soiling accretion and its effect on PV performance by simplified time-series models [23]. A careful method of the defect detection and diagnosis methods used in PV systems has determined the trade-offs in terms of precision, complexity, and deployability [24]. Experimentally-based data-driven modelling has been combined with distance-based classifiers to detect faults in the PV [25].

Early efforts on automatic fault detection in grid connected PV systems developed early foundations of monitoring and diagnosis that still form the basis of the modern PV inspection approaches [26]. The direct quantitative dependence between spatial illumination non-uniformity in PV images and attenuation caused by illumination has not been properly studied. To address this gap, the present study proposes an explainable image-based framework that models PV panel images as two-dimensional illumination fields and quantifies illumination non-uniformity using physically interpretable measures. The proposed method offers a clear and computationally efficient alternative of evaluating the performance of PVs without turning

to electrical measurements or learning-based models by developing a monotonic relationship between illumination non-uniformity and an image-derived attenuation measure.

1.1 Novelty of the Proposed Work

The novelty of the work consists in the physics-directed, pixel-based quantification of attenuation induced by illumination of photovoltaic panels without using electrical and segmentation measurements and learning models. This work, in contrast to image-based studies that are currently in existence, directly, continuously, and monotonically relate spatial illumination non-uniformity to attenuation severity. One of the innovations is the development of a composite index of illumination non-uniformity which incorporates illumination distortion in the frequency domain, spatial discontinuity, and global intensity dispersion as a single analytical instrument. Furthermore, without sensor measurements or training procedures, the attenuation measure based on images provides a physically consistent approximation of performance degradation to aid in the quantitative evaluation of performance. The suggested framework is completely explainable, deterministic, and computationally lean, which provides a clear alternative to data-driven solutions but has high correlation with attenuation behaviour.

2. Methodology

The proposed framework estimates illumination-induced attenuation in photovoltaic panels from the spatial non-uniformity of panel images.

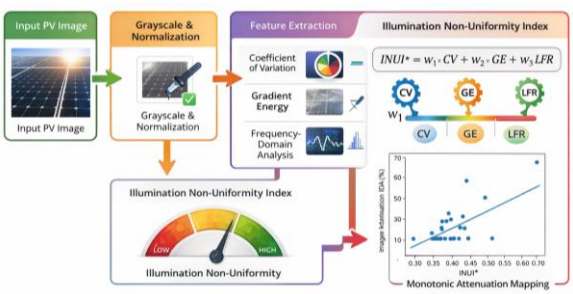

Figure 1. Summary of the suggested image-based non-uniformity analysis technique of photovoltaic attenuation estimation

The approach to the process considers every photovoltaic picture to be a two-dimensional light field and calculates a physically meaningful index of illumination non-uniformity with the assistance of statistical, spatial and frequency domain characteristics. An attenuation measure based on the image is then determined and a monotonic mapping is put between the proposed index and the attenuation measure. Fig. 1 represents the conceptual illustration of the overall workflow of the proposed approach.

2.1 Image pre-processing

Let $G(x,y)$ represent an RGB image of a photovoltaic panel acquired under field conditions. A standard linear transformation is used to convert the image to first a grayscale luminance representation $G(x,y)$, in equation (1), so as to preserve the illumination information,

$$G(x,y)=0.299R(x,y)+0.587G(x,y)+0.144B(x,y) \quad (1)$$

To make the image resistant to the variations in camera exposures and lighting, the grayscale image is normalized to a range of [0,1] as

$$G(x,y)=\frac{G(x,y)-\min(G)}{\max(G)-\min(G)} \quad (2)$$

A mild Gaussian smoothing operation is used to remove high-frequency noise as well as leave behind dominant illumination structures. The resultant image $G(x,y)$ in the equation below (2) is treated as a two-dimensional illumination field representing the relative spatial illumination distribution across the photovoltaic panel.

2.2 Illumination Non-Uniformity Descriptors

Non-uniform illumination is seen in the form of global differences in intensity, sudden spatial changes and broad striping patterns. To identify these attributes, three descriptors are derived out of the normalized illumination field which are complementary.

2.2.1 Global Illumination Variation

The coefficient of variation is used to measure the variation in global illumination, and is given by, standard deviation/ mean intensity,

$$CV = \frac{\sigma_{\hat{G}}}{\mu_{\hat{G}}} \tag{3}$$

In which $\mu_{\hat{G}}$ and $\sigma_{\hat{G}}$ in equation (3) represent the average and the standard deviation of $G(x,y)$ respectively. Smaller CV values indicate more uniform illumination, whereas larger values indicate greater dispersion of illumination intensity associated with non-uniform shading.

2.2.2 Spatial Discontinuity Measure

Gradient-based analysis describes abrupt changes in light caused by material distributions or shadows. The magnitude of gradient of the illumination field, in Equation (4), is computed as,

$$\left|\nabla G(x,y)\right| = \sqrt{\left(\frac{\partial \hat{G}}{\partial x}\right)^2 + \left(\frac{\partial \hat{G}}{\partial y}\right)^2} \tag{4}$$

The spatial discontinuity measure is defined as the normalized mean gradient energy in Equation (5):

$$GE = \frac{\mathbf{E}\left[\left|\nabla G\right|\right]}{\mu_G} \tag{5}$$

This measure captures localized illumination changes caused by partial shading patterns.

2.2.3 Frequency-Domain Distortion of illumination

Large-scale shading regions generate low-frequency distortions in the illumination field. To capture this effect, a two-dimensional discrete cosine transform (DCT) is applied in Equation (6):

$$F(u,v) = DCT\left\{G(x,y)\right\} \tag{6}$$

The ratio of illumination distortion in the low frequency of the equation (7) is given as,

$$LFR = \frac{\sum_{(u,v)\in\Omega_{low}} |F(u,v)|^2}{\sum_{u,v} |F(u,v)|^2} \tag{7}$$

where the specified region represents the low-frequency components surrounding the direct-current (DC) component. The LFR descriptor captures smooth, spatially extended shading effects that may not be adequately represented by local intensity statistics alone.

2.3 Illumination Non-Uniformity Index

The illumination non-uniformity index combines the complementary information provided by the three descriptors is shown in Table 1. In order to combine complementary information presented by the three descriptors, all the components are normalized with the help of min-max scaling on the whole dataset. Then, the index of the illumination non-uniformity is defined as a weighted mean,

$$INUI = \alpha CV_n + \beta GE_n + \gamma LFR_n \tag{8}$$

Table 1. Definition of the illumination non-uniformity descriptors of the proposed framework

Descriptor	Symbol	Description
Coefficient of variation	(CV)	Global illumination intensity dispersion
Gradient energy	(GE)	Spatial illumination discontinuity
Low-frequency ratio	(LFR)	Large-scale illumination distortion
Illumination non-uniformity index	(INUI*)	Weighted composite illumination index

where CV_n, GE_n and LFR_n in equation (8) represent the normalized descriptors, and $\alpha+\beta+\gamma=1$. The weighting coefficients were selected empirically to provide balanced contributions from the three complementary descriptors. A slightly higher weight (0.40) was assigned to the gradient energy descriptor because localized illumination discontinuities caused by partial shading have a more pronounced influence on attenuation than global intensity variations or low-frequency illumination distortions. The coefficient of variation and low-frequency ratio were each assigned equal weights (0.30) to preserve balanced representation of global illumination dispersion and large-scale shading patterns. No formal optimization or sensitivity analysis was performed in the present study, as the primary objective was to establish a physically interpretable and deterministic image-based attenuation framework.

2.4 Image-Derived Attenuation Metric

To enable quantitative assessment of illumination attenuation using only RGB images, an image-derived attenuation metric is formulated as a physically interpretable surrogate indicator. Rather than directly estimating the electrical power output of a photovoltaic module, the proposed metric quantifies the relative reduction in effective illumination with respect to a uniformly illuminated reference panel. Since the photocurrent generated by a photovoltaic module is fundamentally governed by the spatial distribution of incident irradiance, variations in image-derived illumination provide a meaningful approximation of attenuation severity. Consequently, the proposed attenuation metric is intended to represent relative illumination-induced performance degradation and serves as an explainable image-based indicator rather than a direct substitute for electrical measurements. The usable irradiance fraction is approximated as shown in Equation (9):

$$I_u = \frac{1}{N}\sum_{x,y} G(x,y) \tag{9}$$

The corresponding image-derived percentage attenuation is then expressed as shown in Equation (10):

$$IDA(\%) = 100\left(1 - \frac{I_u}{\mu_{clean}}\right) \tag{10}$$

The metric therefore provides a continuous and physically consistent proxy for illumination-induced attenuation.

2.5 Monotonic Attenuation Estimation Model

The Monotonic Attenuation Estimation model uses estimation, prediction, and control methods. The relationship between the illumination non-uniformity index and the image-derived attenuation metric is represented using a monotonic linear mapping, as shown in Equation (11):

$$IDA = m.INUI + c \tag{11}$$

where the parameters are obtained through least-squares fitting. The monotonic formulation ensures physically meaningful behaviour; whereby greater illumination non-uniformity is associated with greater attenuation. The proposed process does not involve learning-based models or defect-classification mechanisms.

3. Data Description and Experimental Set Up

The image dataset, experimental setup, preprocessing parameters, and evaluation procedure that were utilized to validate the suggested lighting non-uniformity analysis framework are described in this part.

3.1 Image Dataset Description

The experimental evaluation was conducted using a dataset comprising 90 RGB images of photovoltaic modules acquired under real outdoor operating conditions. The dataset was intentionally designed to encompass representative illumination scenarios encountered in practical photovoltaic installations, including clean modules, dust accumulation, partial shading, mixed shading patterns, and non-uniform illumination caused by environmental obstructions. Unlike learning-based approaches that require large annotated datasets for model training, the proposed framework is entirely deterministic and does not involve parameter learning or data-driven optimization. Consequently, the image dataset represented in Fig.2 is employed to evaluate the robustness and consistency of the proposed illumination descriptors rather than to train a predictive model.

(a) Clean/uniform

(b) Dust-induced non-uniformity

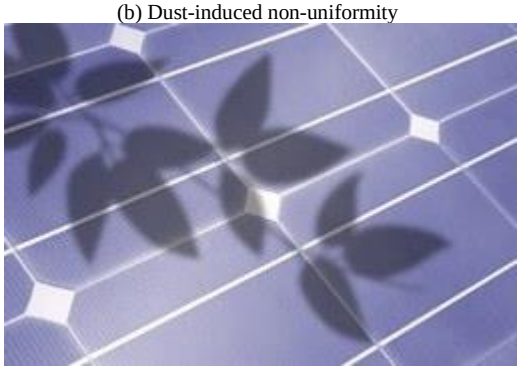

(c) Partial shadow

(d) Mixed shading

(e) Dust-induced gradient

(f) Field-scale non-uniformity

Figure 2. An example of representative photovoltaic panels in different illumination conditions

The selected dataset therefore provides sufficient diversity to validate the physical behaviour of the proposed illumination non-uniformity index across representative attenuation conditions while maintaining a manageable experimental framework. The experimental dataset was acquired using a single photovoltaic module technology under controlled illumination conditions. Consequently, the present validation is limited to one panel configuration.

Although the present study considers ninety representative photovoltaic images, the proposed methodology is inherently independent of dataset size because the feature extraction and attenuation estimation procedures operate on each image individually without prior training. Consequently, the framework can be directly applied to larger image collections acquired from different photovoltaic installations without algorithmic modification. Nevertheless, future investigations will include extensive multi-site datasets covering diverse climatic conditions, module technologies, camera viewpoints, and seasonal variations to further evaluate the scalability and generalizability of the proposed framework.

Table 2. Summary of the image dataset and experimental setup

Item	Description
Number of images	90
Image source	Field-captured PV panel images
Illumination conditions	Clean, dust-affected, partial shading
Image type	RGB, converted to grayscale
Preprocessing	Gaussian smoothing, Normalisation.
Sensors used	None

Consequently, the dataset captures variations in surface reflectance and ambient illumination encountered under field conditions. The non-invasive aspect of the suggested approach is supported by the absence of supplementary sensors or specialized imaging equipment. The nature of the image dataset and the experimental setup followed in this method are summarized in Table 2 including quantity of images, imaging conditions, and preprocessing operations and lack of auxiliary sensors. This overview formulates the practicality and non-invasive character of the suggested image-based framework.

3.2 Image Preprocessing

All the images were transformed to grayscale luminance representations before proceeding to feature extraction after the process in Section 2. Images of grayscale were brought to [0,1] to counter the effects of exposure variation across captures of images. The sensor noise was reduced using a small kernel sized Gaussian smoothing filter that was used to smooth the image without eliminating the dominant illumination structures. No geometrical correction, perspective correction or region of interest segmentation was done. The given design option guarantees that the suggested framework will be simple and entirely image-based, and will not be based on any panel layout data or camera calibration decisions.

3.3 Selection of Reference Illumination

Reference illumination is determined using clean and uniformly illuminated photovoltaic panel images acquired under comparable imaging conditions. In calculating the image-based attenuation parameter, a relative number of images of clean and uniformly lit photovoltaic panels was utilized to provide a reference level of illumination. The mean intensities of these reference images were normalized and averaged to establish the baseline illumination level. The reference value approximates a uniformly illuminated condition without significant shading or surface obstruction. Each of the attenuation estimates was provided in relation to this baseline, without the use of electrical measurements or irradiance sensors, making it possible to compare it to the rest of the dataset.

3.4 Evaluation Protocol

The proposed illumination non-uniformity index was computed for each photovoltaic image following the methodology described in Section 2. The image-derived attenuation metric was subsequently estimated and related to the proposed index using a monotonic linear mapping. The evaluation focused on assessing the consistency, monotonicity, and predictive capability of the proposed index with respect to the image-derived attenuation metric. Because the objective of this work is to develop an explainable image-based attenuation assessment framework, electrical measurements such as current-voltage characteristics or power output were not incorporated into the present validation. Instead, the analysis evaluates whether the proposed illumination descriptors provide a physically meaningful representation of relative illumination attenuation across diverse operating conditions. In addition, rank-based correlation analysis was performed to assess the monotonic relationship independently of linear scaling effects.

3.5 Robustness and Sensitivity Analysis

To evaluate robustness to imaging variations, controlled perturbations were applied to selected images using mild brightness scaling and additive noise. The present robustness analysis focuses on brightness variations and additive noise because these represent the most common photometric disturbances encountered during image acquisition. Although additional practical factors such as camera viewpoint changes, specular reflections, different camera devices, weather conditions, and seasonal illumination variations were not explicitly investigated in the present study, the proposed framework is expected to exhibit reasonable robustness because it relies on normalized illumination descriptors derived from relative spatial intensity distributions rather than absolute pixel values. Nevertheless, comprehensive evaluation under diverse imaging conditions remains an important direction for future work.

4. Results and Discussion

This section presents the experimental findings obtained using the proposed illumination non-uniformity analysis framework and discusses their physical interpretation, robustness, and implications

for photovoltaic performance assessment. The analysis focuses on interpreting the observed patterns from the perspective of illumination distribution rather than relying solely on statistical correlation.

4.1 Relationship between Illumination Non-Uniformity and Attenuation

The proposed illumination non-uniformity index was compared with the image-derived attenuation metric across all 90 photovoltaic panel images acquired under various operating conditions. The results demonstrate a clear monotonic relationship between the index values and attenuation levels, indicating that greater spatial illumination non-uniformity is associated with greater attenuation. The monotonic linear mapping based on the weighted illumination non-uniformity index yielded a coefficient of determination (R^2) of 0.77, indicating that a substantial proportion of the variation in the image-derived attenuation metric can be explained using image-based illumination characteristics alone. The obtained results indicate that the proposed illumination non-uniformity index consistently captures variations in spatial illumination associated with attenuation severity using image-derived information alone. Although electrical measurements were not incorporated into the present validation, the observed monotonic relationship demonstrates that physically interpretable image descriptors can effectively characterize relative illumination attenuation. Therefore, the proposed framework is intended as an explainable image-based assessment tool that complements conventional electrical characterization by enabling rapid visual estimation of attenuation severity. Table 3 summarizes the quantitative performance of the proposed illumination non-uniformity index across the complete image dataset.

Table 3. Performance of the proposed illumination non-uniformity index for image-derived attenuation estimation

Metric	Value
Coefficient of determination (R^2)	0.77
Mean absolute error (%)	9.44
Root mean square error (%)	12.54
Number of samples	90

4.2 Contribution of Individual Illumination Descriptors

To determine the relative contribution of each descriptor, the image-derived attenuation metric was analysed independently against each component of the illumination non-uniformity index. The coefficient of variation primarily represents global intensity variation caused by uneven surface coverage and gradual illumination gradients, such as those associated with dust deposition. The gradient energy measure captures spatial illumination discontinuities associated with shadow edges and partial obstruction. On the other hand, because it makes use of the low-frequency information in the illumination field, the frequency-domain description reacts to smooth, spatially diffuse shading patterns that affect the panel's vast area. The plots of the relations between the attenuation metric and the respective individual descriptors are shown in Fig. 3.

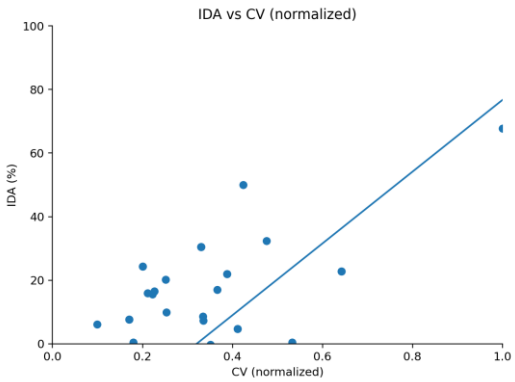

(a) coefficient of variation

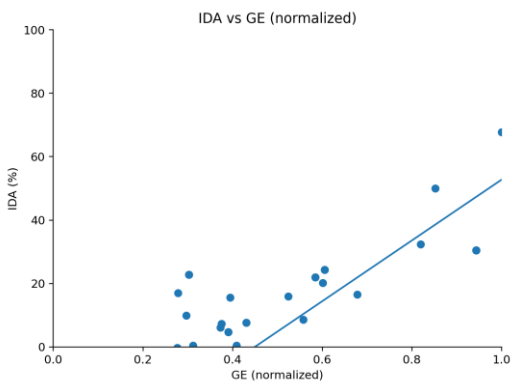

(b) gradient energy

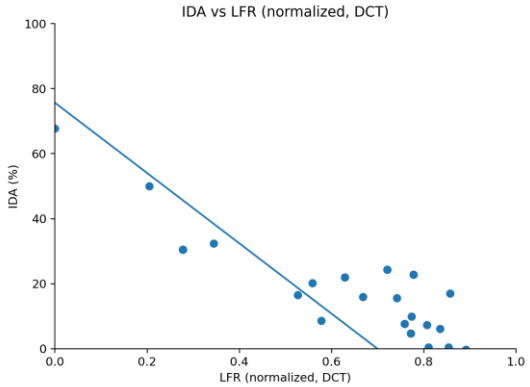

(c) low-frequency distortion ratio

Figure 3. Relationship between the image-derived attenuation metric and individual illumination non-uniformity descriptors: (a) coefficient of variation, (b) gradient energy, and (c) low-frequency distortion ratio

Fig. 3(a) shows how attenuation responds to variation in global intensity, Fig. 3(b) shows the role of sharp spatial transition and Fig. 3(c) shows that there is a strong correlation between attenuation and low-frequency distortion of illumination. The frequency-domain descriptor exhibits a pronounced relationship with attenuation, highlighting the influence of large-area shading on the image-derived attenuation metric. The overall illumination non-uniformity index integrates complementary statistical, spatial, and frequency-domain information from the individual descriptors. This complementary representation provides the rationale for constructing the composite index using the selected weighting scheme.

4.3 Effect of Index Reweighting

The effect of reweighting the illumination non-uniformity index is illustrated in Fig. 4, where the performance of the original index is compared with the selected reweighted formulation. The reweighting procedure strengthens the monotonic relationship and reduces the estimation error.

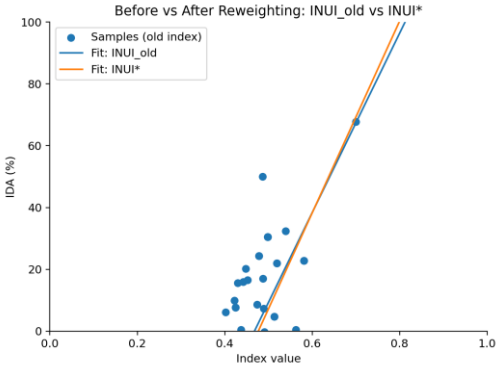

Figure 4. Comparison of attenuation estimation performance before and after reweighting of the illumination non-uniformity index

4.4 Residual Analysis and Model Behavior

The residual behaviour of the proposed monotonic attenuation estimation model is illustrated in Fig. 5. Figure 5(a) presents the residuals as a function of the illumination non-uniformity index, while Fig. 5(b) shows the residual distribution.

The deviations are symmetrically spread around the zero throughout the entire index range, which implies that there is neither systematic overestimation nor underestimation at certain light conditions. No clear systematic change in residual spread is visually observed across the evaluated index range, suggesting broadly consistent estimation behaviour across the tested attenuation levels.

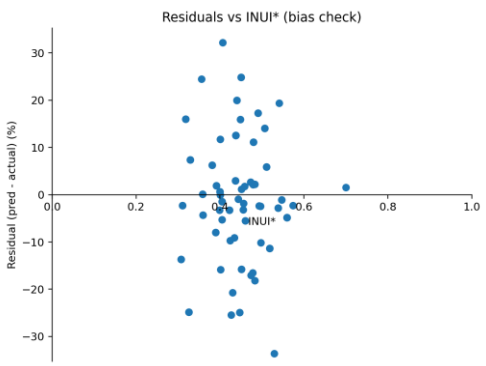

(a) residuals versus illumination non-uniformity index

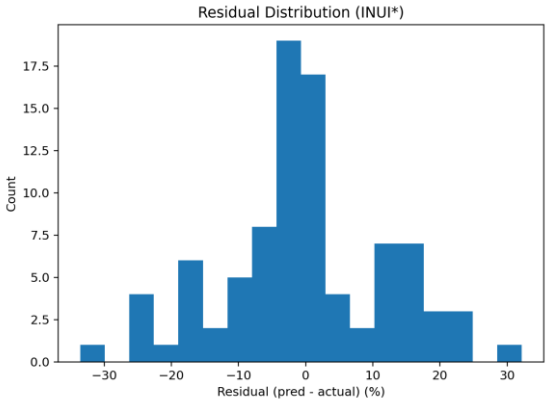

(b) residual distribution

Figure 5. Residual analysis of the proposed monotonic attenuation estimation model: (a) residuals versus the illumination non-uniformity index and (b) residual distribution

This behaviour supports the assumed physically consistent relationship between illumination non-uniformity and attenuation severity and the suitability of the selected monotonic linear mapping.

In addition to the quantitative performance metrics (R^2, MAE, and RMSE), the residual distribution and residual-versus-index analysis were examined to assess the reliability of the proposed attenuation estimation framework. As illustrated in Fig. 5, the residuals are distributed approximately symmetrically around zero without exhibiting a systematic trend with respect to the attenuation index. This behaviour indicates the absence of significant estimation bias across the evaluated attenuation range and demonstrates that the proposed framework provides consistent prediction performance over the experimental dataset.

4.5 Robustness to Imaging Variations

The stability of the proposed illumination non-uniformity index under brightness variation and additive noise is demonstrated in Fig. 6. The close correspondence between the index values obtained from the original images and their perturbed counterparts indicates robustness to common photometric variations such as exposure changes and sensor noise. This strength is important in real-world application, which is because the PV images taken under outdoor conditions are exposed to uncontrollable phenomenon like light, camera controls, and environmental disruptions.

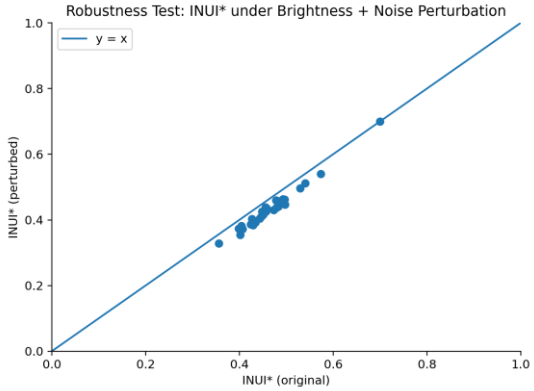

Figure 6. Robustness of the proposed illumination non-uniformity index under brightness and noise perturbations

The stability of the descriptors indicates that they primarily capture structural illumination characteristics rather than short-term photometric artefacts, supporting their potential applicability to practical monitoring conditions. Furthermore, the robustness evaluation under combined brightness variation and additive noise demonstrates that the perturbed attenuation index closely follows the original index values, indicating stable estimation behaviour under representative imaging perturbations.

4.5.1 Practical Imaging Considerations

Beyond brightness variation and additive noise, practical photovoltaic inspection may involve changes in viewing geometry, camera characteristics, environmental reflections, atmospheric conditions, and seasonal illumination variations. Since the proposed framework employs grayscale normalization together with statistical, spatial, and frequency-domain illumination descriptors, moderate photometric variations are expected to have limited influence on the extracted features. However, significant perspective distortions, strong specular reflections, or extreme environmental conditions may affect the spatial illumination distribution and consequently influence attenuation estimation. These practical challenges were beyond the scope of the present study and will be systematically investigated using larger multi-device and multi-season image datasets in future work.

4.6 Computational Efficiency and Deployment Scalability

The proposed framework was implemented on a CPU-based computing platform using standard image-processing operations. For an input image of size *H*W*, preprocessing and extraction of the coefficient of variation, gradient energy, and low-frequency ratio require a single traversal or transform over the image domain, resulting in an overall computational complexity of approximately *O (HW)*. The subsequent illumination non-uniformity index calculation and linear attenuation mapping require only constant-time arithmetic operations with a complexity of *O (1)*, as shown in Table 4.

The average execution time for preprocessing and feature extraction was approximately 1.98 ms per image, while index computation and monotonic attenuation mapping each required approximately 0.01 ms. Therefore, the complete computational pipeline required approximately 2.00 ms per image on the tested CPU platform. This timing excludes image acquisition, file-transfer, and communication delays. The low execution time, absence of iterative model inference, and lack of training requirements indicate that the framework is potentially suitable for real-time implementation on conventional CPUs and resource-constrained edge platforms.

For large-scale photovoltaic installations, the computational workload increases approximately linearly with the number of processed images. Since each image is analysed independently, the framework can also be parallelized across processor cores, edge nodes, or distributed inspection units.

Table 4. Computational complexity and average execution time

Processing stage	Complexity	Average time per image	Remarks
Preprocessing and CV/GE/LFR extraction	**O(HW)**	**1.979 ms**	**CPU-based; no training**
INUI* computation	**O(1)**	**0.010 ms**	**Weighted arithmetic sum**
Linear attenuation mapping	**O(1)**	**0.010 ms**	**Single linear operation**
Complete computational pipeline	**O(HW)**	**≈ 2.00 ms**	**Excludes capture and communication**

However, deployment-scale performance will additionally depend on image resolution, image-acquisition frequency, storage requirements, communication bandwidth, and the selected edge-device hardware. Validation on embedded platforms and large photovoltaic arrays will therefore form part of future work.

4.7 Discrimination across Attenuation Levels

Fig. 7 demonstrates the values of the index of non-uniformity in the distribution of illumination over the various attenuation ranges. As attenuation increases, the distribution and median of the index values show a steady upward trend, with distinct separation between the low- and high-attenuation regimes. This monotonic behavior demonstrates the discriminative capability of the proposed index without requiring explicit classification, thresholding, or rule-based decision logic.

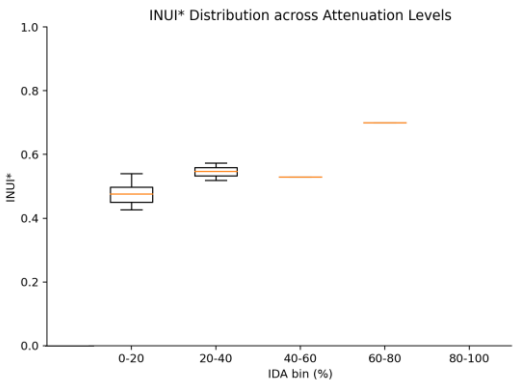

Figure 7. Distribution of illumination non-uniformity index values across different attenuation ranges

Continuous severity measurements of this type are of great benefit to the use of PV performance monitoring systems, in the context of which periodic degradation progressions are often more likely to be relevant than fault classifications.

4.8 Implementation and Practical Applicability

The computational complexity of the proposed framework is very low, only based on the basic image processing operations and linear mapping. Without training, model storage, or parameter modification, the CPU-based implementation performs feature extraction and index computation within a few milliseconds per image. Table 5 summarizes the detailed breakdown of computation.

Table 5. Computational cost of the suggested image-based estimation of attenuation framework

Stage	Time per	Remarks

	image	
Preprocessing	~1–2 ms	Grayscale and smoothing
Descriptor extraction	~2 ms	CV, GE, DCT-based LFR
Index computation	<0.1 ms	Weighted summation
Attenuation mapping	<0.1 ms	Linear model

The low computational cost and non-intrusive image acquisition approach support the scalability of the framework for large-scale photovoltaic monitoring and periodic inspection using low-cost imaging platforms.

Although the experimental evaluation was conducted using a single photovoltaic module type, the proposed attenuation estimation framework is fundamentally based on image-derived illumination descriptors rather than technology-specific electrical characteristics. The extracted features, including the coefficient of variation, gradient energy, and low-frequency ratio, quantify spatial illumination non-uniformity independently of photovoltaic material composition. Consequently, the proposed methodology is expected to be applicable to different photovoltaic technologies, including monocrystalline, polycrystalline, thin-film, and bifacial modules, provided that the captured images adequately represent the visible illumination distribution. Nevertheless, comprehensive validation across multiple photovoltaic technologies and module architectures remains an important direction for future work.

4.9 Comparison with Existing Approaches

Table 6 compares the proposed framework with representative image-based and machine learning-based photovoltaic attenuation estimation methods reported in the literature. Conventional electrical methods require dedicated sensors and electrical measurements for attenuation assessment, whereas most recent image-based approaches rely on supervised learning models for defect classification or segmentation.

Table 6 Comparison of the proposed framework with existing photovoltaic attenuation estimation approaches

Method	**Electrical Sensors**	**Machine Learning**	**Explainable**	**Training Required**	**Computational Complexity**	**Quantitative Attenuation Estimation**
I–V based methods	✓	✗	✓	✗	Medium	✓
CNN-based methods	✗	✓	✗	✓	High	Mostly classification
U-Net segmentation	✗	✓	Partial	✓	High	Segmentation only
RGB image classification	✗	✓	Partial	✓	Medium	Mostly categorical
Proposed Method	✗	✗	✓	✗	Low	✓

These methods generally require extensive labelled datasets, model training, and computational resources, while their decision-making process is often difficult to interpret. In contrast, the proposed framework employs deterministic image-processing descriptors derived from illumination statistics, spatial discontinuity, and frequency-domain characteristics. Consequently, it does not require labelled datasets, model training, or parameter optimization. Furthermore, the proposed method provides a continuous and physically interpretable attenuation indicator instead of categorical defect labels, making it particularly suitable for rapid visual assessment and deployment on computationally constrained platforms.

5. Advantages of the Proposed Approach

The proposed framework offers several practical and technical advantages:

1. **Non-invasive and sensorless:** The approach uses conventional photographic images and does not require electrical measurements, irradiance sensors, or thermal imaging devices.
2. **Physically realistic and intuitive:** The individual components of the illumination non-uniformity index can be interpreted in terms of global illumination variation, shadow edges, and spatial illumination non-uniformity.
3. **No training or labelled datasets:** Unlike conventional deep learning approaches, the proposed framework directly computes deterministic illumination descriptors from RGB images and therefore eliminates the need for labelled datasets,

iterative model training, hyperparameter optimization, and periodic retraining.

4. **Computational efficiency:** The feature extraction and index computation involve lightweight image-processing operations that can be efficiently executed on a conventional CPU-based computer.

5. **Stability to imaging distortions:** The framework demonstrates robustness to the moderate brightness variations and additive noise evaluated in the present study.

6. **Scalability and deployability:** The low computational cost and modest hardware requirements support potential large-scale deployment using low-cost cameras or unmanned inspection platforms.

6. Future Scope

Although the present work focuses on illumination-induced attenuation analysis using static images, several extensions can be considered in future studies. Temporal variations in shading and illumination can be investigated using sequential images acquired over time. Hybrid frameworks combining explainable image processing with data-driven models may also be developed using the proposed illumination non-uniformity index to improve estimation accuracy while preserving interpretability. Furthermore, integration with electrical and environmental measurements can enable multimodal validation and calibration across different photovoltaic technologies. For large-scale solar-farm inspection, the framework can potentially be extended to airborne or oblique imaging platforms, including unmanned aerial vehicles. These extensions could broaden the applicability of the proposed approach for large-scale photovoltaic system monitoring and attenuation assessment.

7. Conclusion

This paper introduced a non-invasive image-based framework for analysing illumination non-uniformity and estimating attenuation in photovoltaic modules. A physically interpretable illumination non-uniformity index was developed by modelling panel images as two-dimensional illumination fields using statistical, spatial, and frequency-domain descriptors. An image-derived attenuation metric was formulated to establish a monotonic relationship between illumination patterns and attenuation severity without requiring electrical measurements or learning-based models. Experimental evaluation across diverse photovoltaic images demonstrated a clear monotonic relationship between the proposed index and the image-derived attenuation metric. The proposed framework provides an explainable, computationally efficient, and scalable approach for assessing illumination-induced attenuation using conventional RGB images. Rather than replacing conventional electrical characterization, the proposed method complements existing inspection practices by enabling rapid visual assessment of attenuation severity from image information alone. Compared with existing learning-based photovoltaic image analysis methods, the proposed framework provides a transparent, computationally lightweight, and training-free alternative for quantitative attenuation assessment while preserving physical interpretability. Future work will focus on validating the proposed image-derived attenuation metric against measured electrical characteristics, including current-voltage (I–V) curves, output power, and irradiance, across different photovoltaic technologies and environmental conditions.

Acknowledgements

The authors gratefully acknowledge the management of Thiagarajar College of Engineering for providing financial support through the Thiagarajar Research Fellowship (TRF) scheme (File No. TCE/RD/TRF/July2024/07), which supported this research work.

Nomenclature

α, β, γ	Weighting coefficients assigned to the individual illumination non-uniformity descriptors
c	Intercept of the monotonic linear mapping
CV	Coefficient of variation
DC	Direct-current component
DCT	Discrete cosine transform
$F(u,v)$	Two-dimensional DCT coefficient at spatial-frequency coordinates (u,v)
$G(x,y)$	RGB image of the photovoltaic panel at spatial coordinates (x,y)
GE	Gradient energy
H	Image height
$I(x,y)$	Grayscale illumination intensity at

	spatial coordinates (x,y)
IDA	Image-derived attenuation
INUI	Illumination non-uniformity index
*INUI**	Weighted illumination non-uniformity index
I–V	Current–voltage
LFR	Low-frequency ratio
m	Slope of the monotonic linear mapping
MAE	Mean absolute error
N	Number of photovoltaic panel images used for evaluation
PV	Photovoltaic
R^2	Coefficient of determination
RGB	Red, green, and blue
RMSE	Root mean square error
UAV	Unmanned aerial vehicle
W	Image width
x, y	Spatial coordinates in the image
u, v	Spatial-frequency coordinates in the DCT domain
μ	Mean intensity of the normalized illumination field
σ	Standard deviation of the normalized illumination field

References

[1] Abdelsattar, M., AbdelMoety, A., & Emad-Eldeen, A. (2025). ResNet-based image processing approach for precise detection of cracks in photovoltaic panels. *Scientific Reports*, *15*, 24356. https://doi.org/10.1038/s41598-025-09101-z

[2] Araji, M. T., & Waqas, A. (2025). Integrated deep learning and image processing method for modeling energy loss due to shadows in solar arrays. *Solar Energy*, *297*, 113623. https://doi.org/10.1016/j.solener.2025.113623

[3] Naeem, U., et al. (2025). Aerial imaging-based soiling detection system for solar photovoltaic panel cleanliness inspection. *Sensors*, *25*(3), 738. https://doi.org/10.3390/s25030738

[4] Ahmed, S., et al. (2025). Deep learning-based recognition and classification of soiled photovoltaic modules using HALCON software for solar cleaning robots. *Sensors*, *25*(5), 1295. https://doi.org/10.3390/s25051295

[5] Chen, L., et al. (2025). A detection model for dust deposition on photovoltaic (PV) panels based on light transmittance estimation. *Energy*, *322*, 135284. https://doi.org/10.1016/j.energy.2025.135284

[6] Özüpak, Y. (2025). Real-time detection of photovoltaic module faults using a hybrid machine learning model. *Solar Energy*, *302*, 114014. https://doi.org/10.1016/j.solener.2025.114014

[7] Agbogla, J., et al. (2025). Soiling estimation methods in solar photovoltaic systems: Review, challenges and future directions. *Results in Engineering*, *26*, 104810. https://doi.org/10.1016/j.rineng.2025.104810

[8] Tao, Y., Yu, T., & Yang, J. (2025). Photovoltaic array fault diagnosis and localization method based on modulated photocurrent and machine learning. *Sensors*, *25*(1), 136. https://doi.org/10.3390/s25010136

[9] Rudro, R. A. M., et al. (2024). SPF-Net: Solar panel fault detection using U-Net based deep learning image classification. *Energy Reports*, *12*, 1580–1594. https://doi.org/10.1016/j.egyr.2024.07.044

[10] Amiri, A. F., Kichou, S., Oudira, H., Chouder, A., & Silvestre, S. (2024). Fault detection and diagnosis of a photovoltaic system based on deep learning using the combination of a convolutional neural network and bidirectional gated recurrent unit. *Sustainability*, *16*(3), 1012. https://doi.org/10.3390/su16031012

[11] Winkel, P., et al. (2024). Cell-resolved PV soiling measurement using drone images. *Remote Sensing*, *16*(14), 2617. https://doi.org/10.3390/rs16142617

[12] Evstatiev, B. I., et al. (2024). PV module soiling detection using visible spectrum imaging and machine learning. *Energies*, *17*(20), 5238. https://doi.org/10.3390/en17205238

[13] Setiawan, E. A., et al. (2024). Fast partial shading detection on PV modules for precise power loss ratio estimation using digital image processing. *Journal of Electrical and Computer Engineering*, *2024*, 9385602. https://doi.org/10.1155/2024/9385602

[14] Sarkar, S., et al. (2024). A model for effect of partial shading on PV panels with experimental validation. *Energy Reports*, *12*, 3460–3469. https://doi.org/10.1016/j.egyr.2024.09.015

[15] Lin, W.-T., Chang, C.-M., Huang, Y.-C., Wu, C.-C., & Kuo, C.-C. (2024). Fault diagnosis in solar array I–V curves using characteristic simulation and multi-input models. *Applied Sciences*, *14*(13), 5417. https://doi.org/10.3390/app14135417

[16] Puppala, H., Maganti, L. S., Peddinti, P. R. T., & Motapothula, M. R. (2024). Thermographic inspections of solar photovoltaic plants in India using unmanned aerial vehicles: Analysing the gap between theory and practice. *Renewable Energy*, *237*(Part B), 121694. https://doi.org/10.1016/j.renene.2024.121694

[17] Eesaar, H., et al. (2023). SEiPV-Net: An efficient deep learning framework for autonomous multi-defect segmentation in electroluminescence images of solar photovoltaic modules. *Energies*, *16*(23), 7726. https://doi.org/10.3390/en16237726

[18] Duranay, Z. B. (2023). Fault detection in solar energy systems: A deep learning approach. *Electronics*, *12*(21), 4397. https://doi.org/10.3390/electronics12214397

[19] Cavieres, R., Barraza, R., Estay, D., Bilbao, J., & Valdivia-Lefort, P. (2022). Automatic soiling and partial shading assessment on PV modules through RGB image analysis. *Applied Energy*, *306*, 117964. https://doi.org/10.1016/j.apenergy.2021.117964

[20] Bessa, J. G., et al. (2021). Monitoring photovoltaic soiling: Assessment, challenges, and perspectives of current and potential strategies. *iScience*, *24*(3), 102165. https://doi.org/10.1016/j.isci.2021.102165

[21] Deitsch, S., et al. (2021). Segmentation of photovoltaic module cells in uncalibrated electroluminescence images. *Machine Vision and Applications*, *32*, 84. https://doi.org/10.1007/s00138-021-01191-9

[22] Gao, W., & Wai, R.-J. (2020). A novel fault identification method for photovoltaic array via convolutional neural network and residual gated recurrent unit. *IEEE Access*, *8*, 159493–159510. https://doi.org/10.1109/ACCESS.2020.3020296

[23] Coello, M., & Boyle, L. (2019). Simple model for predicting time series soiling of photovoltaic panels. *IEEE Journal of Photovoltaics*, *9*(5), 1382–1387. https://doi.org/10.1109/JPHOTOV.2019.2919628

[24] Mellit, A., Tina, G. M., & Kalogirou, S. A. (2018). Fault detection and diagnosis methods for photovoltaic systems: A review. *Renewable and Sustainable Energy Reviews*, *91*, 1–17. https://doi.org/10.1016/j.rser.2018.03.062

[25] Madeti, S. R., & Singh, S. N. (2018). Modeling of PV system based on experimental data for fault detection using kNN method. *Solar Energy*, *173*, 139–151. https://doi.org/10.1016/j.solener.2018.07.038

[26] Silvestre, S., Chouder, A., & Karatepe, E. (2013). Automatic fault detection in grid-connected PV systems. *Solar Energy*, *94*, 119–127. https://doi.org/10.1016/j.solener.2013.05.001